

Chapter 15

Locking Free High-Order Mixed Elements for Ferroelectric Polarization



Astrid S. Pechstein, Martin Meindlhumer, Alexander Humer,
and Michael Krommer

Abstract In this contribution, a finite element discretization for a thermodynamically consistent macroscopic model of the ferroelectric polarization process is introduced. Usually, finite elements are based on an incremental optimization problem for the electric enthalpy, and displacement and electric potential are the degrees of freedom of choice. Less common, energy-based models involving displacement and dielectric displacement have been proposed. In this work, the model is reformulated in terms of the mechanic enthalpy, leading to stress and dielectric displacement as independent unknowns. Choosing stable pairs of mixed finite elements for the mechanic and the electric quantities, a locking-free finite element method of arbitrary order is designed. Numerical results show the robustness of the method.

15.1 Introduction

The piezoelectric effect allows to convert electric loads into mechanical deformations and vice versa. Modern piezoceramics provide high precision actuation and sensing at moderate cost. In order to exhibit the piezoelectric effect, these ceramics have to be polarized initially by a high electric field. In most applications, it is assumed that the consequent remanent polarization state is unidirectional and constant, which leads essentially to Voigt's theory of linear piezoelectricity [22]. However, the remanent polarization state can change under different—sufficiently high—mechanical

A. S. Pechstein (✉) · M. Meindlhumer · A. Humer · M. Krommer
Institute of Technical Mechanics, Johannes Kepler University Linz, Altenberger Str. 69, 4040
Linz, Austria
e-mail: astrid.pechstein@jku.at

M. Meindlhumer
e-mail: martin.meindlhumer@jku.at

A. Humer
e-mail: alexander.humer@jku.at

M. Krommer
e-mail: michael.krommer@jku.at

© The Author(s), under exclusive license to Springer Nature Switzerland AG 2022
H. Irschik et al. (eds.), *Dynamics and Control of Advanced Structures and Machines*,
Advanced Structured Materials 156,
https://doi.org/10.1007/978-3-030-79325-8_15

or electrical loadings. On the other hand, for involved geometries as occurring in macro-fiber composites (MFCs), the applied poling electric field does not lead to a unidirectional polarization state. For these reasons, the numerical simulation of the polarization process and of mechanic and electric depolarization is an active field of research.

In this work, a phenomenological description of the macroscopic material behavior is adopted. The remanent polarization state is considered as an internal variable, similar to the plastic strain in elastoplasticity. The proposed model is thermodynamically consistent. The first to suggest such thermodynamically consistent models were the group around Maugin [1–4]. McMeeking and Landis [9], as well as Schröder and Romanowski [19] provided models including a remanent polarization strain depending directly on the remanent polarization. However, these models are still capable of mechanical depolarization. Independent polarization strains were considered, e.g., by Landis [7] or Klinkel [6].

An extensive introduction on variational frameworks for these models is provided by Miehe et al. [12]. In their work, energy and electric enthalpy-based models are considered. These different models require different sets of free unknowns. Most classical finite element methods are electric enthalpy based, where displacement (or strain) and electric potential (or electric field) are the primary unknowns. Few methods are energy-based with displacement and dielectric displacement as independent unknowns. We cite a vector potential model by Semenov et al. [20] and a one-dimensional model by Sands and Guz [18]. An energy-based method involving mixed finite elements was suggested by Pechstein et al. [16, 17].

The present work deals with a model based on the mechanic enthalpy. Stress and dielectric displacement are the primary unknowns of this model. For both the mechanical and the electrical quantities, stable pairs of mixed elements are employed. The major benefit of this approach is the fact that the mixed mechanic elements are locking free with respect to shear locking for flat elements. We choose *tangential displacement normal-normal stress* (TDNNS) elements, which were used in the context of simulation of linear piezoelectric materials by Pechstein et al. [15] and Meindlhumer et al. [10, 11]. Thus, these elements are well designed for the discretization of flat piezoelectric patches or thin integrated structures. The electric mixed elements were designed by Lehrenfeld and Schöberl [8] such that Gauss' law of zero charges is satisfied exactly.

15.2 Thermodynamic Model

Let $\Omega \subset \mathbb{R}^3$ denote the domain of interest. We introduce the quantities of interest in our electromechanically coupled model. First, $\mathbf{u} : \Omega \rightarrow \mathbb{R}^3$ shall denote the displacement field. We assume to stay in small-strain regime, where the linearized strain tensor $\mathbf{S} = \frac{1}{2}(\nabla \mathbf{u} + (\nabla \mathbf{u})^T)$ is used. Its work conjugate is the symmetric total stress tensor \mathbf{T} . For the electric quantities, we introduce the electric potential $\varphi : \Omega \rightarrow \mathbb{R}$ and the electric field as its negative derivative, $\mathbf{E} = -\nabla \varphi$. Its work conjugate is the

dielectric displacement vector denoted by \mathbf{D} . In the following, we will refer to displacement \mathbf{u} and electric potential φ as well as strain \mathbf{S} and electric field \mathbf{E} as *primal* quantities, whereas the stress tensor \mathbf{T} and dielectric displacement \mathbf{D} are referred to as *dual* quantities. Ferroelectric polarization is described by a further macroscopic field, the remanent polarization \mathbf{P}^i . In this contribution, we assume that the remanent polarization \mathbf{P}^i directly accounts for the polarization strain $\mathbf{S}^i = \mathbf{S}^i(\mathbf{P}^i)$ due to the smaller computational complexity of such a formulation.

The conjugate, dual quantities \mathbf{T} and \mathbf{D} both satisfy balance equations

$$-\operatorname{div} \mathbf{T} = \mathbf{f} \quad \text{and} \quad -\operatorname{div} \mathbf{D} = 0, \quad (15.1)$$

where \mathbf{f} denotes the given volume loads. Additionally, boundary conditions have to be satisfied. For the mechanic quantities, we assume the body is fixed on some part Γ_{fix} and free on the remaining part $\Gamma_{\text{free}} = \partial\Omega \setminus \Gamma_{\text{fix}}$. Moreover, we assume that the electric potential is prescribed on some part of the boundary Γ_{pot} , whereas the body is insulated elsewhere on $\Gamma_{\text{ins}} = \partial\Omega \setminus \Gamma_{\text{pot}}$,

$$\mathbf{u} = 0 \quad \text{on } \Gamma_{\text{fix}} \quad \text{and} \quad \mathbf{T} \cdot \mathbf{n} = 0 \quad \text{on } \Gamma_{\text{free}}, \quad (15.2)$$

$$\varphi = V_0 \quad \text{on } \Gamma_{\text{pot}} \quad \text{and} \quad \mathbf{D} \cdot \mathbf{n} = 0 \quad \text{on } \Gamma_{\text{ins}}. \quad (15.3)$$

Primal and dual quantities are related to each other via the material law. We assume a thermodynamically consistent material model, which is described by a thermodynamic potential. For a detailed introduction, we refer to Miehe et al. [12], in the following, we provide a short presentation of enthalpy-based material modeling.

Usually, a potential representing the electric enthalpy of the system is given, where the primal unknowns and the remanent polarization are the free variables,

$$\Psi_e = \int_{\Omega} \psi_e(\mathbf{S}, \mathbf{E}, \mathbf{P}^i) \, dx. \quad (15.4)$$

Above, we used the convention that the lower-case expression ψ_e denotes the density of the upper-case potential Ψ_e . Then, stress and dielectric displacement are defined as (negative) derivatives of the potential density with respect to strain and electric field

$$\mathbf{T} = \frac{\partial \psi_e}{\partial \mathbf{S}}, \quad \mathbf{D} = -\frac{\partial \psi_e}{\partial \mathbf{E}}. \quad (15.5)$$

While Ψ_e corresponds to the energy stored in the system, the dissipated energy is represented by the dissipation function Φ . The dissipation function depends only on the rate of the irreversible polarization, and is again defined via a density function

$$\Phi(\dot{\mathbf{P}}^i) = \int_{\Omega} \phi(\dot{\mathbf{P}}^i) \, dx. \quad (15.6)$$

We assume that the dissipation function is positively homogeneous, which corresponds to rate-independent behavior (see also [12])

$$\phi(\alpha \dot{\mathbf{P}}^i) = \alpha \phi(\dot{\mathbf{P}}^i) \quad \text{for all } \alpha \geq 0. \quad (15.7)$$

With the above ingredients, for any time interval $[t_0, t_1]$, the following incremental optimization problem has to be satisfied

$$\Psi(t_1) - \Psi(t_0) + \int_{t_0}^{t_1} \Phi(\dot{\mathbf{P}}^i) dt + \int_{t_0}^{t_1} P_{\text{ext}} dt \rightarrow \min_{\mathbf{S}(\mathbf{u})} \max_{\mathbf{E}=-\nabla\varphi} \min_{\mathbf{P}^i} \quad (15.8)$$

Above, the work of external forces \mathbf{f} is included in the external power by defining

$$P_{\text{ext}} = \int_{\Omega} \mathbf{f} \cdot \dot{\mathbf{u}} dx. \quad (15.9)$$

So far, only well-known contributions from the literature have been reviewed. In the following, we propose to use the mechanic enthalpy Ψ_m of the system instead of the electric enthalpy Ψ_e . Then, the dual quantities \mathbf{T} and \mathbf{D} are free variables. The mechanic enthalpy is related to the electric enthalpy via a Legendre transformation in the following way; see e.g. [21]

$$\Psi_m(\mathbf{T}, \mathbf{D}, \mathbf{P}^i) = \min_{\mathbf{S}(\mathbf{u})} \max_{\mathbf{E}=-\nabla\varphi} \Psi_e(\mathbf{S}, \mathbf{E}, \mathbf{P}^i) - \int_{\Omega} \mathbf{T} : \mathbf{S} dx + \int_{\Omega} \mathbf{D} \cdot \mathbf{E} dx. \quad (15.10)$$

In the simple case of potentials quadratic in strain and electric field, this transformation can be computed in the standard way: assume the electric enthalpy density ψ_e is of the standard form

$$\begin{aligned} \psi_e = & \frac{1}{2} (\mathbf{S} - \mathbf{S}^i(\mathbf{P}^i)) : \mathbf{C}_E : (\mathbf{S} - \mathbf{S}^i(\mathbf{P}^i)) \\ & + (\mathbf{S} - \mathbf{S}^i(\mathbf{P}^i)) : \mathbf{e} \cdot \mathbf{E} \\ & - \frac{1}{2} \mathbf{E} \cdot \epsilon_S \cdot \mathbf{E} - \mathbf{P}^i \cdot \mathbf{E} + \psi_i(\mathbf{P}^i) \end{aligned} \quad (15.11)$$

where all material moduli \mathbf{C}^E , \mathbf{e} and ϵ^S may depend on the remanent polarization state \mathbf{P}^i , and where $\psi_i(\mathbf{P}^i)$ denotes an additional hardening term. Then the mechanic enthalpy is given by the relation

$$\begin{aligned} \psi_m = & -\frac{1}{2} \mathbf{T} : \mathbf{S}_D : \mathbf{T} - \mathbf{T} : \mathbf{g} \cdot (\mathbf{D} - \mathbf{P}^i) \\ & + \frac{1}{2} (\mathbf{D} - \mathbf{P}^i) \cdot \beta_T \cdot (\mathbf{D} - \mathbf{P}^i) \\ & - \mathbf{S}^i(\mathbf{P}^i) : \mathbf{T} + \psi_i(\mathbf{P}^i). \end{aligned} \quad (15.12)$$

The material moduli are connected to each other via

$$\begin{aligned}
\mathbf{C}_E &= (\mathbf{S}_E)^{-1}, \\
\mathbf{S}_D &= \mathbf{S}_E - \mathbf{d}^T \cdot \beta_T \cdot \mathbf{d}, \\
\beta_T &= (\epsilon_T)^{-1}, \\
\epsilon_S &= \epsilon_T - \mathbf{d} : \mathbf{C}_E : \mathbf{d}^T, \\
\mathbf{e} &= \mathbf{d} : \mathbf{C}_E, \\
\mathbf{g} &= \beta_T \cdot \mathbf{d}.
\end{aligned} \tag{15.13}$$

An optimization problem equivalent to (15.8) can be posed

$$\Psi_m(t_1) - \Psi_m(t_0) + \int_{t_0}^{t_1} \Phi(\dot{\mathbf{P}}^i) dt \rightarrow \max_{-\operatorname{div} \mathbf{T}=\mathbf{f}} \min_{-\operatorname{div} \mathbf{D}=0} \min_{\mathbf{P}^i}. \tag{15.14}$$

Note that, in comparison to (15.8), the work of external forces \mathbf{f} is now not included in P_{ext} , but

$$-\operatorname{div} \mathbf{T} = \mathbf{f} \tag{15.15}$$

is posed as constraint. Lagrangian multipliers may be introduced enforcing these constraints. We define the Lagrangian \mathcal{L}

$$\mathcal{L}(\mathbf{T}, \mathbf{D}, \mathbf{P}^i, \mathbf{u}, \varphi) = \Psi_m(\mathbf{T}, \mathbf{D}, \mathbf{P}^i) - \int_{\Omega} \mathbf{u} \cdot (\operatorname{div} \mathbf{T} + \mathbf{f}) dx - \int_{\Omega} \varphi \operatorname{div} \mathbf{D} dx. \tag{15.16}$$

The corresponding optimization problem for the Lagrangian \mathcal{L} reads

$$\mathcal{L}(t_1) - \mathcal{L}(t_0) + \int_{t_0}^{t_1} \Phi(\dot{\mathbf{P}}^i) dt \rightarrow \max_{\mathbf{T}} \min_{\mathbf{D}} \min_{\mathbf{u}} \max_{\varphi} \min_{\mathbf{P}^i}. \tag{15.17}$$

Above, \mathbf{u} and φ have been introduced as Lagrangian multipliers. It shows that indeed they resemble the primal kinematic quantities displacement and electric potential.

15.3 Discretization

15.3.1 Semidiscretization in Time

We consider a discretization of the time interval $[0, T]$ into (not necessarily equal-sized) time steps $\{t_i\}_{i=0\dots N}$, such that $t_0 = 0$ and $t_N = T$. We propose a time stepping scheme, where we assume at some time t_{n-1} all quantities known. We use

$\mathbf{u}_{n-1} = \mathbf{u}(t_{n-1})$ etc. as an abbreviation. Let $\Delta t = t_n - t_{n-1}$ denote the time step size. Approximating the remanent polarization rate by the quotient $\dot{\mathbf{P}}^i \simeq (\mathbf{P}_n^i - \mathbf{P}_{n-1}^i)/\Delta t$, we observe for positively homogeneous dissipation functions Φ that

$$\int_{t_{n-1}}^{t_n} \Phi(\dot{\mathbf{P}}^i) dt = \Phi(\mathbf{P}_n^i - \mathbf{P}_{n-1}^i). \quad (15.18)$$

The optimization problem corresponding to (15.17) for this time step transforms into the problem of finding \mathbf{T}_n , \mathbf{u}_n and \mathbf{D}_n , φ_n , \mathbf{P}_n^i such that

$$\begin{aligned} \mathcal{L}(\mathbf{T}_n, \mathbf{D}_n, \mathbf{P}_n^i, \mathbf{u}_n, \varphi_n) - \mathcal{L}(\mathbf{T}_{n-1}, \mathbf{D}_{n-1}, \mathbf{P}_{n-1}^i, \mathbf{u}_{n-1}, \varphi_{n-1}) + \Phi(\mathbf{P}_n^i - \mathbf{P}_{n-1}^i) \\ \rightarrow \max_{\mathbf{T}_n} \min_{\mathbf{D}_n} \min_{\mathbf{u}_n} \max_{\varphi_n} \min_{\mathbf{P}_n^i} . \end{aligned} \quad (15.19)$$

Together with a suitable choice of finite element bases, the variation of the above optimization problem leads to a system of nonlinear variational equations, that can be solved by a Newton-Raphson iteration.

15.3.2 Spatial Finite Element Discretization

The finite element discretization of the optimization problem for the Lagrangian (15.19) has to be done with care. Stable families of finite elements have to be chosen for the electric quantities \mathbf{D} and φ as well as the mechanic quantities \mathbf{T} and \mathbf{u} . Both pairs have to satisfy an inf-sup condition for the respective divergence operators, which will be discussed in the following.

Below, we assume that $\mathcal{T} = \{T\}$ is a regular finite element mesh of the domain Ω . The mesh \mathcal{T} may contain tetrahedral, prismatic and hexahedral elements, but must be free from hanging nodes. Due to the choice of discretization, flat prismatic or hexahedral elements suitable for the discretization of plates or shells are admissible without additional mechanical locking effects.

15.3.2.1 Discretization of the Electrical Quantities

When analyzing the different terms of the optimization problem (15.19), one notes that different differentiability requirements for \mathbf{D} and φ are required as compared to standard problems. The divergence of the dielectric displacement, $\text{div } \mathbf{D}$, has to be computed, while no derivatives of the electric potential φ are evaluated. This is a standard feature of mixed methods. In choosing finite elements for \mathbf{D} and φ , two requirements have to be met:

- the dielectric displacement \mathbf{D} has to be divergence conforming, i.e., $D_n = \mathbf{D} \cdot \mathbf{n}$ has to be continuous across element boundaries, and
- dielectric displacement \mathbf{D} and electric potential φ have to satisfy an inf-sup condition, i.e., there exists some constant c independent of the mesh size such that

$$\inf_{\varphi} \sup_{\mathbf{D}} \frac{\int_{\Omega} \varphi \operatorname{div} \mathbf{D} \, dx}{\|\mathbf{D}\|_{H(\operatorname{div})} \|\varphi\|_{L^2}} \geq c. \quad (15.20)$$

We will not dwell any longer on these issues. The interested reader is referred to the exhaustive monograph by Boffi, Brezzi, and Fortin [5] for theoretical background on mixed problems. As a first choice, one could use standard mixed finite elements for the electrical quantities

$$\mathbf{D} \in \mathbf{V}_D := \{\mathbf{D} : \mathbf{D}|_T \in [P^k(T)]^3, D_n \text{ continuous}\}, \quad (15.21)$$

$$\varphi \in \mathbf{V}_{\varphi} := \{\varphi : \varphi|_T \in P^k(T)\}. \quad (15.22)$$

Using the notation of [5], this is the Brezzi-Douglas-Marini space \mathcal{BDM}_k for the dielectric displacement, as well as a discontinuous polynomial space for the electric potential. In [17], we discussed that the number of degrees of freedom can be reduced significantly if one considers that $\operatorname{div} \mathbf{D} = 0$. Although this condition is non-local, Lehrenfeld and Schöberl [8] showed that it is possible to eliminate at least the high-order contributions locally on the element level. They designed a reduced set of basis functions, such that the $\operatorname{div} \mathbf{D}$ is at most constant per element. For this reduced set of basis functions, a smaller number of Lagrangian multipliers (i.e. electric potential φ basis functions) is necessary to enforce $\operatorname{div} \mathbf{D} = 0$. The finite element spaces are reduced to

$$\mathbf{D} \in \mathbf{V}_{D,red} := \{\mathbf{D} : \mathbf{D}|_T \in [P^k(T)]^3, \operatorname{div} \mathbf{D}|_T \in P^0(T), D_n \text{ continuous}\}, \quad (15.23)$$

$$\varphi \in \mathbf{V}_{\varphi,red} := \{\varphi : \varphi|_T \in P^0(T)\}. \quad (15.24)$$

15.3.2.2 Discretization of the Mechanical Quantities

In a mixed method comparable to Sect. 15.3.2.1, one would expect stress elements with continuous stress vector $\mathbf{T}_n = \mathbf{T} \cdot \mathbf{n}$ at element interfaces, whereas the displacement vector is allowed to be discontinuous. Such methods are difficult to design, but usually free from shear locking. For an overview on the mathematical properties of mixed methods in elasticity; see [5].

In the current contribution, we use the mixed finite element method introduced by Pechstein and Schöberl in [13]. There, only the normal component of the stress vector $T_{nn} = \mathbf{n} \cdot \mathbf{T} \cdot \mathbf{n}$ is continuous, which makes it easier to design conforming symmetric finite element basis functions. Complementarily, the tangential component of the displacement vector $\mathbf{u}_t = \mathbf{u} - (\mathbf{u} \cdot \mathbf{n})\mathbf{n}$ is continuous, and gaps between elements

may open up only in normal direction. For straight simplicial elements, the finite element spaces are

$$\mathbf{T} \in \mathbf{V}_T := \{\mathbf{T} : \mathbf{T}|_T \in [P^k(T)]_{sym}^{3 \times 3}, T_{nn} \text{ continuous}\}, \quad (15.25)$$

$$\mathbf{u} \in \mathbf{V}_u := \{\mathbf{u} : \mathbf{u}|_T \in [P^k(T)]^3, \mathbf{u}_t \text{ continuous}\}. \quad (15.26)$$

For prismatic, hexahedral or curved elements, the definition of the spaces is more complex and addressed in [10, 14].

As such, the stress tensor is not divergence conforming. In other words, the work pair

$$\int_{\Omega} \operatorname{div} \mathbf{T} \cdot \mathbf{u} \, dx \quad (15.27)$$

cannot be evaluated as an integral, but has to be understood in distributional sense. It contains volume terms on each element, and additionally element boundary terms including the jumping tangential component of the stress vector $\mathbf{T}_{nt} = \mathbf{T} \cdot \mathbf{n} - (\mathbf{n} \cdot \mathbf{T} \cdot \mathbf{n})\mathbf{n}$. For a thorough discussion, we refer to the earlier works [13, 15]. For completeness, we provide the definition of the distributional divergence operator for the tangential continuous finite element function \mathbf{u} and normal-normal continuous \mathbf{T} by

$$\langle \operatorname{div} \mathbf{T}, \mathbf{u} \rangle_{\Omega} := \sum_{T \in \mathcal{T}} \left(\int_T \operatorname{div} \mathbf{T} \cdot \mathbf{u} \, dx - \int_{\partial T} \mathbf{T}_{nt} \cdot \mathbf{u}_t \, ds \right) \quad (15.28)$$

$$= - \sum_{T \in \mathcal{T}} \left(\int_T \mathbf{S}(\mathbf{u}) : \mathbf{T} \, dx - \int_{\partial T} T_{nn} u_n \, ds \right) = - \langle \mathbf{S}(\mathbf{u}), \mathbf{T} \rangle_{\Omega}. \quad (15.29)$$

Note that, also in this distributional sense, divergence and strain operator are dual. In both (15.28) and (15.29), on the element interfaces, the continuous finite element function (\mathbf{u}_t or T_{nn} , respectively) acts as a Lagrangian multiplier enforcing continuity of their discontinuous counterpart (\mathbf{T}_{nt} or u_n , respectively).

15.3.2.3 Discretization of the Remanent Polarization

The remanent polarization can be discretized in a completely independent way. It does not need to satisfy any continuity assumptions, as no derivatives of \mathbf{P}^i occur in the variational equations. To be of consistent order, we propose to use piecewise polynomial elements for \mathbf{P}^i that are of the same order as the dielectric elements,

$$\mathbf{P}^i \in \mathbf{V}_P := \{\mathbf{P}^i : \mathbf{P}^i|_T \in [P^k(T)]^3\}. \quad (15.30)$$

15.4 Numerical Results

We present a benchmark example taken from Semenov et al. [20]. A quadratic plate of size $l = 20\text{mm} \times 20\text{mm}$ and thickness $h = 6\text{mm}$ has a circular hole of diameter $d = 4\text{mm}$ through its center. Choosing the xy plane as the in-plane direction, it is electroded at $x = 0$ and $x = l$. By applying a potential of $\pm\varphi_0 = \pm 15000\text{V}$ to the electrodes an electric field is induced in in-plane x direction. Singularities evolve around the circular hole. Due to symmetry, only one eighth of the plate is modeled by finite elements.

The plate is made from PZT-5H, which is modeled in the following way using the parameters from Table 15.1: the mechanic enthalpy is chosen as in (15.12). Electric permittivity at constant stress $\beta_T = 1/\epsilon_T \mathbf{I}$ is assumed isotropic constant. The piezoelectric tensor \mathbf{d} depends on the remanent polarization as in [7], such that it reflects the d_{31} and d_{33} effect. The flexibility at constant dielectric displacement is chosen as

$$\mathbf{S}_D = \mathbf{S}(Y_E, \nu) - 0.6 \mathbf{d}^T \cdot \beta_T \cdot \mathbf{d}, \quad (15.31)$$

as for this choice

$$\mathbf{S}_E = \mathbf{S}_D + \mathbf{d}^T \cdot \beta_T \cdot \mathbf{d} \quad (15.32)$$

is close to the anisotropic tensor found in material databases. There, $\mathbf{S}(Y_E, \nu)$ denotes the standard isotropic flexibility tensor for given Young's modulus Y_E and Poisson ratio ν . Concerning ferroelectric hardening and saturation, the additive energy ψ_i in (15.12) is chosen such that its derivative is

$$\begin{aligned} \psi'_i(\mathbf{P}^i) &= \tilde{\psi}'_i(|\mathbf{P}^i|) \frac{\mathbf{P}^i}{|\mathbf{P}^i|} \\ \text{with } \tilde{\psi}'_i(r) &= \frac{h_0 P_0^m}{2(m-1)} \left((P_0 - r)^{1-m} - (P_0 + r)^{1-m} \right) \end{aligned} \quad (15.33)$$

The remanent polarization strain, that depends fully on the remanent polarization, is given as proposed by McMeeking and Landis [9]

$$\mathbf{S}(\mathbf{P}^i) = \frac{3}{2} \frac{S_0}{P_0^2} \left(\mathbf{P}^i \mathbf{P}^i - \frac{1}{3} (\mathbf{P}^i \cdot \mathbf{P}^i) \mathbf{I} \right). \quad (15.34)$$

Finally, the dissipation function contains the coercive electric field, and describes the onset of switching. Its density is defined as

$$\phi(\dot{\mathbf{P}}^i) = E_0 |\dot{\mathbf{P}}^i|. \quad (15.35)$$

This choice is motivated in detail in [16]. As discussed in [17], the additive energy ψ_i and the dissipation function are regularized by a small parameter $\varepsilon = 10^{-4} P_0$.

Table 15.1 Material parameters for PZT-5H, see also [20]

Young's modulus Y_E	$61 \times 10^9 \text{Nm}^{-2}$
Poisson ratio ν	0.31
el. permittivity ϵ_T	$2.77 \times 10^{-8} \text{Fm}^{-1}$
Piezoelectric d_{31}	$2.74 \times 10^{-10} \text{mV}^{-1}$
Piezoelectric d_{33}	$5.93 \times 10^{-10} \text{mV}^{-1}$
Coercive electric field E_0	$820 \times 10^3 \text{Vm}^{-1}$
Hardening parameter h_0	$714 \times 10^3 \text{mF}^{-1}$
Saturation polarization P_0	0.24Cm^{-2}
Saturation strain S_0	9.3×10^{-3}
Shape parameter m	1.4

The additive energy is modified such that its second derivative of ψ_i stays bounded as $|\mathbf{P}^i|$ approaches saturation, whereas the dissipation function is approximated by a differentiable function. We use

$$\psi'_{i,\varepsilon}(\mathbf{P}^i) = \begin{cases} \psi'_i(\mathbf{P}^i) & \text{if } |\mathbf{P}^i| \leq P_0 - \varepsilon, \\ (\tilde{\psi}'_i(P_0 - \varepsilon) + \tilde{\psi}''_i(P_0 - \varepsilon)(|\mathbf{P}^i| - \varepsilon + P_0)) \frac{\mathbf{P}^i}{|\mathbf{P}^i|} & \text{if } |\mathbf{P}^i| > P_0 - \varepsilon \end{cases} \quad (15.36)$$

$$\phi_\varepsilon = E_0 \sqrt{|\mathbf{P}^i|^2 + \varepsilon^2}. \quad (15.37)$$

In the original reference [20], the voltage was raised from zero to 15000V in several load steps. For our formulation, we found that we could use as little as four load steps and still observe convergence of a Newton iteration with linesearch. Note that such a low number of load steps may impede accuracy in case of non-proportional loading. However, in the present benchmark the focus lies on iteration numbers and maximum loadstep size. In Table 15.2, we present the iteration counts for different finite element orders, using prismatic meshes.

For the first three results, there was no refinement of the prismatic mesh in thickness z -direction, resulting in an overall count of 95 elements. For the latter three results, we used three elements over thickness, see e.g. Fig. 15.1 for the two different discretizations. We compare our values to the counts given by [20], where one layer of hexahedral elements was used.

To highlight the accuracy of the method, we compare the results for the lowest resolution (one layer of finite elements of order $k = 1$) to the highest resolution (three layers of order $k = 3$). In the former case, the mesh consisted of 95 elements, 10 184 overall degrees of freedom were obtained, of which 2 864 were coupling, while in the latter case we had 179 631 degrees of freedom of which 35 931 were coupling. Figure 15.1 shows the remanent polarization $|\mathbf{P}^i|$ at $\Delta V = 15000\text{V}$, and Fig. 15.2 shows the corresponding electric field.

Table 15.2 Iteration counts for the plate with hole

	5000 V	8000 V	10000 V	15000 V
Semenov [20]	5	6	27 (5 incr)	29 (6 incr)
One layer				
$k = 1$	8	11	29	27
$k = 2$	10	12	39	28
$k = 3$	14	14	48	31
Three layers				
$k = 1$	9	13	32	26
$k = 2$	10	16	34	29
$k = 3$	14	14	47	44 (2 incr)

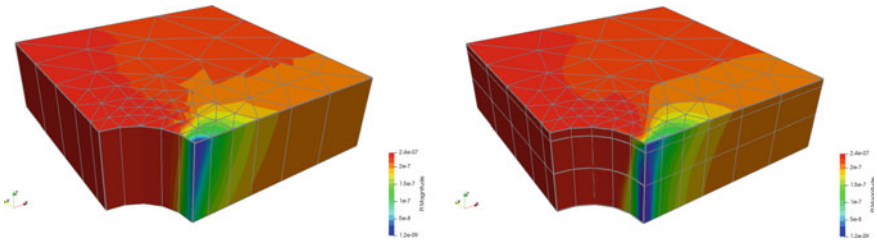


Fig. 15.1 Remanent polarization $|P^i|$ (unit MC/m^2) for the coarsest discretization (one layer of prismatic elements of order $k = 1$) and the finest discretization (three layers of elements of order $k = 3$)

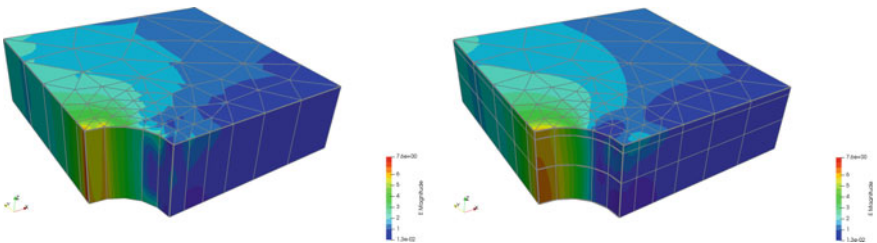


Fig. 15.2 Electric field $|E|$ (unit MV/m) for the coarsest discretization (one layer of prismatic elements of order $k = 1$) and the finest discretization (three layers of elements of order $k = 3$)

In Figs. 15.3 and 15.4, the longitudinal stress component T_{xx} as well as the in-plane shear stress component T_{xy} are depicted. Note that in all plots, no stress reconstruction or smoothing was done, the fields are displayed directly as they were computed. The absolute value of the electric field over the central line $x = 0, y \in [2, 10 \text{ mm}], z = 0$ is displayed in Fig. 15.5.

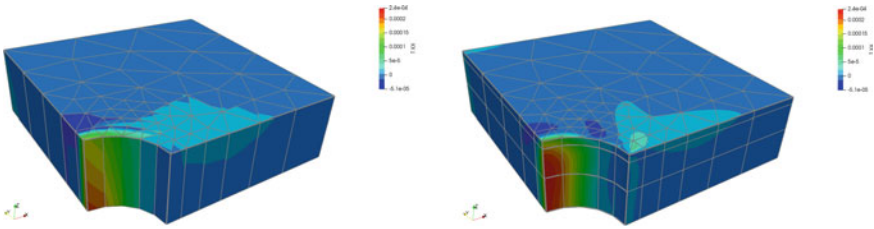


Fig. 15.3 Longitudinal stress component T_{xx} (unit $N/(\mu m)^2$) for the coarsest discretization (one layer of prismatic elements of order $k = 1$) and the finest discretization (three layers of elements of order $k = 3$)

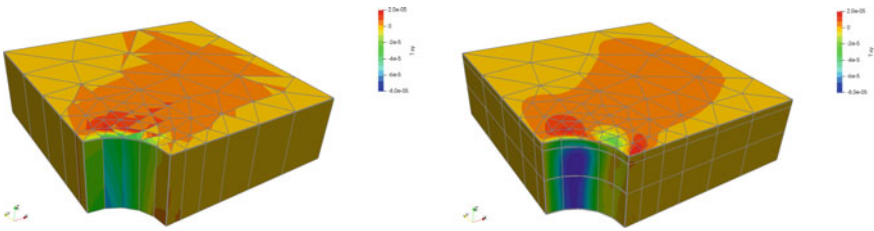
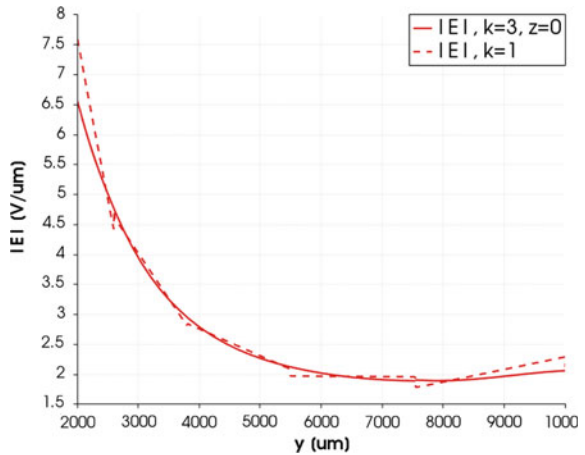


Fig. 15.4 In-plane shear stress component T_{xy} (unit $N/(\mu m)^2$) for the coarsest discretization (one layer of prismatic elements of order $k = 1$) and the finest discretization (three layers of elements of order $k = 3$)

Fig. 15.5 Absolute value of the electric field $|\mathbf{E}|$ over the central line $x = 0$, $y \in [2, 10 \text{ mm}]$, $z = 0$ for the two different discretizations with $k = 1$ and $k = 3$



15.5 Conclusion

A finite element method for a mechanic enthalpy-based model of the ferroelectric polarization process has been presented. In such a model, dielectric displacement and stress are the primary unknowns. Two stable pairs of mixed finite elements were chosen to discretize the model. For the electric quantities, divergence-conforming dielectric elements are proposed, such that Gauss' law of zero charges is satisfied exactly. Taking this law into account, the total number of degrees of freedom could even be reduced, choosing only basis functions with at most constant divergence. For the mechanic quantities, mixed TDNNS elements are used, as they have been shown to be free from shear locking when using flat elements in thin layers of piezoelectric structures. By way of a numerical benchmark example, robustness of the method with respect to large load increments is shown.

Acknowledgements Martin Meindlhumer acknowledges support of Johannes Kepler University Linz, Linz Institute of Technology (LIT). This work has been supported by the Linz Center of Mechatronics (LCM) in the framework of the Austrian COMET-K2 program.

References

1. Bassiouny, E., Ghaleb, A., Maugin, G.: Thermodynamical formulation for coupled electromechanical hysteresis effects—I: basic equations. *Int. J. Eng. Sci.* **26**(12), 1279–1295 (1988)
2. Bassiouny, E., Ghaleb, A., Maugin, G.: Thermodynamical formulation for coupled electromechanical hysteresis effects—II: poling of ceramics. *Int. J. Eng. Sci.* **26**(12), 1297–1306 (1988)
3. Bassiouny, E., Maugin, G.: Thermodynamical formulation for coupled electromechanical hysteresis effects—III: parameter identification. *Int. J. Eng. Sci.* **27**(8), 975–987 (1989)
4. Bassiouny, E., Maugin, G.: Thermodynamical formulation for coupled electromechanical hysteresis effects—IV: combined electromechanical loading. *Int. J. Eng. Sci.* **27**(8), 989–1000 (1989)
5. Boffi, D., Brezzi, F., Fortin, M.: *Mixed finite element methods and applications*. Springer Series in Computational Mathematics, vol. 44. Springer, Heidelberg (2013)
6. Klinkel, S.: A phenomenological constitutive model for ferroelastic and ferroelectric hysteresis effects in ferroelectric ceramics. *International Journal of Solids and Structures* **43**(22–23), 7197–7222 (2006)
7. Landis, C.: Fully coupled, multi-axial, symmetric constitutive laws for polycrystalline ferroelectric ceramics. *Journal of the Mechanics and Physics of Solids* **50**(1), 127–152 (2002)
8. Lehrenfeld, C., Schöberl, J.: High order exactly divergence-free hybrid discontinuous galerkin methods for unsteady incompressible flows. *Computer Methods in Applied Mechanics and Engineering* **307**, 339–361 (2016)
9. McMeeking, R., Landis, C.: A phenomenological multi-axial constitutive law for switching in polycrystalline ferroelectric ceramics. *International Journal of Engineering Science* **40**(14), 1553–1577 (2002)
10. Meindlhumer, M., Pechstein, A.: 3D mixed finite elements for curved, flat piezoelectric structures. *Int. J. Smart Nano Mater.* **10**(4), 249–267 (2019). <https://doi.org/10.1080/19475411.2018.1556186>
11. Meindlhumer, M., Pechstein, A., Humer, A.: Variational inequalities for ferroelectric constitutive modelling. *J. Intell. Mater. Syst. Struct.* **32**(3), 317–330 (2021). <https://doi.org/10.1177/1045389X20951252>

12. Miehe, C., Rosato, D., Kiefer, B.: Variational principles in dissipative electro-magneto-mechanics: A framework for the macro-modeling of functional materials. *International Journal for Numerical Methods in Engineering* **86**(10), 1225–1276 (2011)
13. Pechstein, A., Schöberl, J.: Tangential-displacement and normal-normal-stress continuous mixed finite elements for elasticity. *Math. Models Methods Appl. Sci.* **21**(8), 1761–1782 (2011)
14. Pechstein, A., Schöberl, J.: Anisotropic mixed finite elements for elasticity. *Int. J. Numer. Methods Engrg.* **90**(2), 196–217 (2012)
15. Pechstein, A.S., Meindlhumer, M., Humer, A.: New mixed finite elements for the discretization of piezoelectric structures or macro-fiber composites. *J. Intell. Mater. Syst. Struct.* **29**(16), 3266–3283 (2018). <https://doi.org/10.1177/1045389X18781026>
16. Pechstein, A.S., Meindlhumer, M., Humer, A.: The polarization process of ferroelectric materials in the framework of variational inequalities. *ZAMM - J. Appl. Math. Mech. [Zeitschrift für Angewandte Mathematik und Mechanik]* **100**(6), e201900329 (2020). <https://doi.org/10.1002/zamm.201900329>. <https://onlinelibrary.wiley.com/doi/abs/10.1002/zamm.201900329>
17. Pechstein, A.S., Meindlhumer, M., Humer, A.: High-order mixed finite elements for an energy-based model of the polarization process in ferroelectric materials. *J. Intell. Mater. Syst. Struct.* **32**(3), 355–368 (2021). <https://doi.org/10.1177/1045389X20953895>
18. Sands, C.M., Guz, I.A.: Unidimensional model of polarisation changes in piezoelectric ceramics based on the principle of maximum entropy production. *Journal of Engineering Mathematics* **78**(1), 249–259 (2013)
19. Schröder, J., Romanowski, H.: A thermodynamically consistent mesoscopic model for transversely isotropic ferroelectric ceramics in a coordinate-invariant setting. *Archive of Applied Mechanics* **74**(11–12), 863–877 (2005)
20. Semenov, A., Liskowsky, A., Balke, H.: Return mapping algorithms and consistent tangent operators in ferroelectroelasticity. *International Journal for Numerical Methods in Engineering* **81**(10), 1298–1340 (2010)
21. Tichý, J., Erhart, J., Kittinger, E., Privratska, J.: *Fundamentals of piezoelectric sensorics: mechanical, dielectric, and thermodynamical properties of piezoelectric materials*. Springer Science & Business Media (2010)
22. Voigt, W.: *Lehrbuch der Kristallphysik (mit Ausschluß der Kristalloptik)*. Teubner Leipzig (1910)